THE JOURNAL OF PHYSICAL CHEMISTRY Letters

Perspective

pubs.acs.org/JPCL

Ultrathin One- and Two-Dimensional Colloidal Semiconductor Nanocrystals: Pushing Quantum Confinement to the Limit

Anne C. Berends and Celso de Mello Donega*

Condensed Matter and Interfaces, Debye Institute for Nanomaterials Science, Utrecht University, P.O. Box 80 000, 3508 TA Utrecht, The Netherlands

ABSTRACT: Research on ultrathin nanomaterials is one of the fastest developing areas in contemporary nanoscience. The field of ultrathin one- (1D) and two-dimensional (2D) colloidal nanocrystals (NCs) is still in its infancy, but offers the prospect of production of ultrathin nanomaterials in liquid-phase at relatively low costs, with versatility in terms of composition, size, shape, and surface control. In this Perspective, the state of the art in the field is concisely outlined and critically discussed to highlight the essential concepts and challenges. We start by presenting a brief overview of the ultrathin colloidal 1D and 2D semiconductor NCs prepared to date, after which the synthesis strategies and formation mechanisms of both 1D and 2D NCs are discussed. The properties of these low-dimensional materials are then reviewed, with emphasis on the optical properties of luminescent NCs. Finally, the future prospects for the field are addressed.

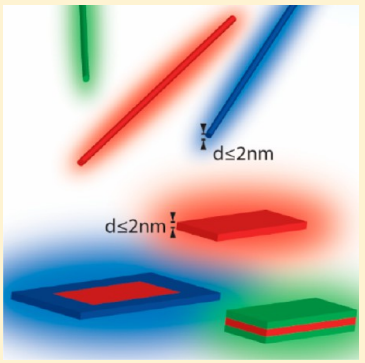

Since its inception nearly four decades ago, the study of colloidal semiconductor nanocrystals (NCs) has matured into a dynamic and multidisciplinary research field, which continues to grow at an outstanding pace.[1−10] This ever-increasing interest stems primarily from the fact that colloidal semiconductor NCs combine size- and shape-dependent optoelectronic properties with easy surface manipulation and solution processing (Figure 1), thereby being promising materials for a myriad of potential applications (light emitting devices, solar cells, luminescent solar concentrators, optoelectronics, sensing, thermoelectrics, biomedical applications, catalysis).[1−10] The intense worldwide research activity that was incited by these prospects resulted in a remarkable degree of control over the composition, size, and shape of colloidal semiconductor NCs, yielding a plethora of zero-dimensional (0D, e.g., cubes, pyramids, quasi-spheres), one-dimensional (1D, e.g., rods, wires), and two-dimensional (2D, e.g., disks, platelets) NCs, as well as more complex morphologies (e.g., multipods).[1−10]

The discovery of the unexpected properties of graphene in 2004[11] generated a surge of research not only on graphene itself, but also on layered 2D materials beyond graphene (e.g., MoS_2, WS_2, and other transition metal dichalcogenides, silicene, phosphorene, boron nitride)[12−15] and colloidal 2D NCs.[15−17] These materials are typically denoted as "ultrathin", a term that is also often used in conjunction with nanowires. Nevertheless, "ultrathin" is an ill-defined concept, as it does not explicitly specify a thickness or diameter range. Very often it is used to indicate a thickness or diameter of just a few atomic monolayers or, in the case of semiconductor nanostructures, dimensions that are sufficiently small to induce strong quantum confinement. The latter is, however, strongly composition dependent, since it is determined by the exciton Bohr radius, which ranges from ∼2 to ∼50 nm depending on the semiconductor.[10] In this Perspective we will define "ultrathin" as the size range corresponding to what is conventionally referred to as the "magic-size regime" ($d \leq 2$ nm), which is characterized by the existence of well-defined atomically precise clusters with an elevated thermodynamic stability compared to slightly smaller or larger ones.[18,19] This definition prevents ambiguities, since it is based on thermodynamically determined size boundaries that are only weakly composition dependent, while encompassing only semiconductor nanostructures that are strongly quantum confined. We will focus on free-standing ultrathin colloidal semiconductor nanowires and nanosheets, as these systems can be seen as quantum wires and quantum wells suspended in low dielectric constant media, free from interactions with a substrate, thereby providing access to the ultimate limits of 2D and 1D quantum confinement. After a brief overview of the ultrathin colloidal 1D and 2D semiconductor NCs prepared to date, we will discuss the synthesis strategies and formation mechanisms proposed for both nanowires and nanosheets. The properties of these low-dimensional nanomaterials will then be reviewed, with emphasis on the optical properties of luminescent ultrathin 1D and 2D colloidal semiconductor NCs. Finally, we will address the future prospects for the field. This Perspective is intended as an enticing overview, in which the state of the art is concisely outlined and critically discussed to highlight the essential challenges that have yet to be addressed. For further details, the interested reader is referred to a number of excellent recent reviews focusing on different aspects of 1D and 2D colloidal semiconductor nanomaterials.[15−17,20,21]

Received: June 26, 2017
Accepted: August 11, 2017
Published: August 11, 2017

DOI: 10.1021/acs.jpclett.7b01640
J. Phys. Chem. Lett. 2017, 8, 4077−4090

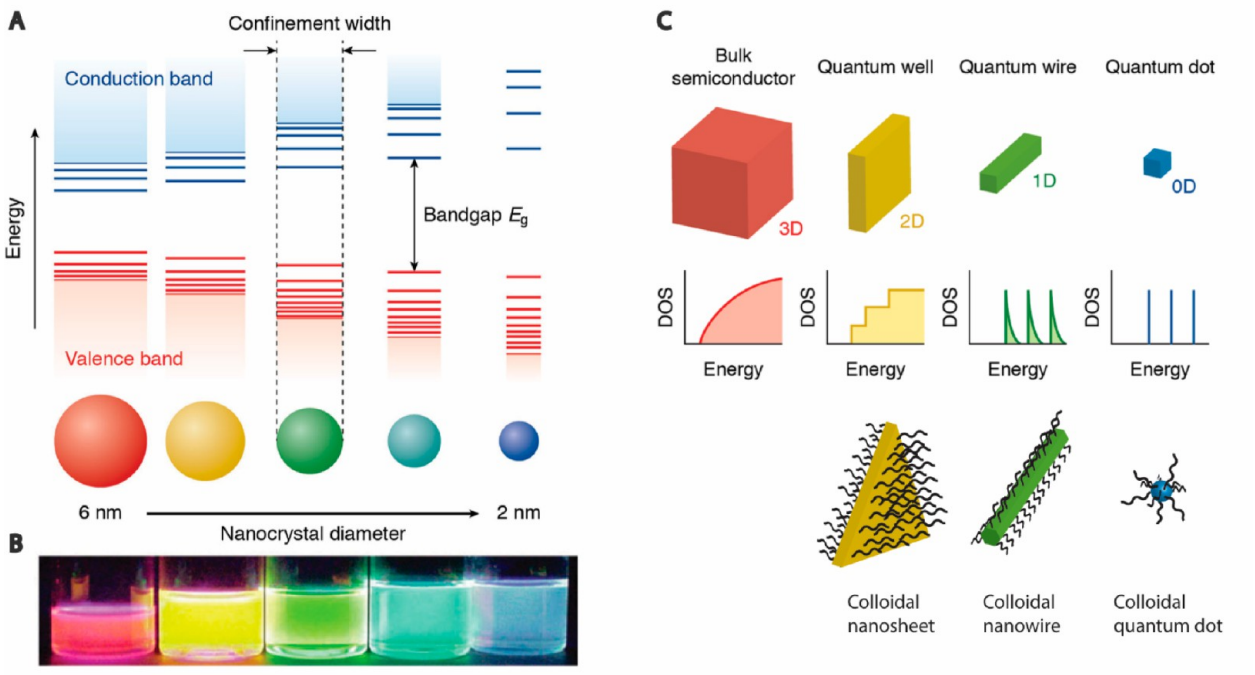

Figure 1. (A) Schematic representation of quantum confinement effects: the bandgap increases and discrete energy levels appear at the band-edges with decreasing nanocrystal size. (B) Colloidal dispersions of CdSe NCs with different sizes, under UV illumination. The NC size decreases from left to right (6 to 2 nm) and the corresponding increase in the bandgap is reflected in the change of the photoluminescence color from red to blue. (C) Schematic representation of the energy level structure of a bulk semiconductor and of semiconductor nanostructures with reduced dimensionality, from 2D (exciton is confined only in the thickness dimension), to 1D (exciton is confined in the diameter direction), to 0D (exciton is confined in all directions) (DOS: density of electronic states). Colloidal NCs capped with organic ligands can be made with dimensionality ranging from 2D to 0D (bottom panel). The ligands have a crucial role during the synthesis and can also be postsynthetically exchanged.[1] Adapted with permission from ref 10. Copyright 2016 Springer International Publishing.

This Perspective is intended as an enticing overview of the field of ultrathin NCs, in which the state of the art is concisely outlined and critically discussed to highlight the essential challenges that have yet to be addressed.

Ultrathin 2D Colloidal Semiconductor Nanocrystals. The recent literature is rich in examples of geometrically 1D and 2D colloidal semiconductor NCs, and many of them are sufficiently thin to exhibit quantum confinement effects.[1,17,20−22] However, ultrathin colloidal NCs of inorganic semiconductors are still restricted to just a few materials, as we will discuss below. Free-standing ultrathin 2D colloidal NCs are referred to in the literature as nanosheets, nanoribbons (or nanobelts), or nanoplatelets, depending on their aspect ratio (and often also on the authors' preference). Nanosheets (NSs) have large in-plane aspect ratios ($L/h \geq 25$, L = lateral dimensions, h = thickness) in all directions and lateral dimensions that are much larger than a_0 ($L < 10\ a_0$), so that in-plane quantum confinement effects can be neglected, making colloidal semiconductor NSs truly 2D systems, and hence ideally suited to investigate 1D-confined excitons. By contrast, nanoribbons and nanobelts (NBs) are characterized by much larger aspect ratios in the length (l) direction than in the width (w) direction ($l/h > 100$, $w/h > 20$, $l/w > 10$), and widths that are often just a few times larger than a_0. NBs are therefore electronically quasi-2D systems, since excitons are not only strongly confined in the thickness direction, but are also still weakly confined in the width direction. Nanoplatelets (NPLs) typically have much smaller aspect ratios than NSs ($L/h > 10$), and are often just a few times larger than a_0, thus being quasi-2D systems as well. As a result, small NPLs can be seen as intermediates between quantum dots (3D-confined excitons) and NSs (1D-confined excitons, i.e. quantum wells), while NBs are intermediates between nanowires (2D-confined excitons) and NSs. It should be noted that the distinction between large NPLs and NSs is only semantic, and therefore some authors use the term "nanoplatelet" rather than "nanosheet" for consistency reasons, so that they can use the same term regardless of the exact aspect ratio.[16,17,22]

To date, ultrathin 2D colloidal NCs of a number of semiconductors have been prepared (Figure 2). The most investigated ones are CdX (X = S, Se, Te) NPLs (h = 1.2−2.1 nm; square or rectangular with irregular edges, L = 10−700 nm, zinc-blende structure)[17,22−24] and NBs (h = 1.4−2.2 nm; $l \leq 1$ μm, w = 10−20 nm, wurtzite structure),[16,25,26] which have been shown to have remarkable optical properties.[16,17,22,23,26] These properties will be discussed in more detail below. Colloidal ZnSe NBs (h = 1.4 nm, l = 40−160 nm, w = 15−30 nm),[27] PbSe NPLs (h = 2 nm, square, $L \sim 50$ nm),[28] PbS NSs (h = 2 nm, square, $L \approx 1$ μm),[29,30] PbS NBs (h = 2 nm; $l \sim 200$ nm, $w \sim 50$ nm),[31] $CsPbBr_3$ NPLs (h = 0.6−3 nm; square or rectangular, L = 20−50 nm),[32,33] and NSs of Sb_2S_3 (h = 1.8 nm; rectangular with ragged edges, L = 100 by 500 nm),[34] SnSe (h = 1 nm, irregularly shaped, L = 300 nm),[35] In_2X_3 (X = S, Se; h = 0.6−1.5 nm, L = 100−900 nm),[36−38] WS_2 (h = 1 nm, irregularly shaped, $L \approx 100$ nm, both 1T and 2H phases but highly defective),[39] $Cu_{2-x}S$ ($x \leq 0.2$, h = 2

DOI: 10.1021/acs.jpclett.7b01640
J. Phys. Chem. Lett. 2017, 8, 4077−4090

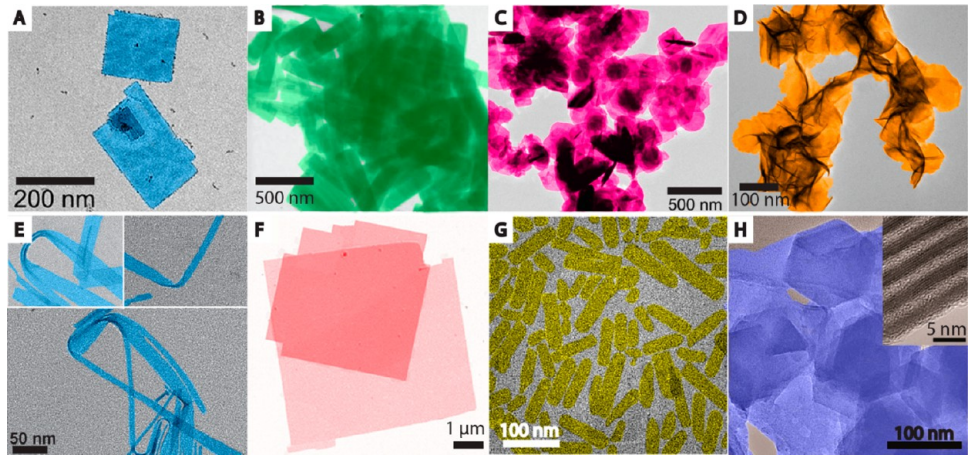

Figure 2. Examples of nanosheets (NSs), nanoplatelets (NPLs) and nanobelts (NBs) of various compositions: (A) square and rectangular CdSe NSs (light blue), (B) Sb_2S_3 NBs (green), (C) SnSe NSs (pink), (D) WS_2 NSs (orange), (E) CdS NBs (light blue), (F) $CsPbBr_3$ perovskite NSs (red), (G) ZnSe NBs (yellow), (H) $Cu_{2-x}S$ NSs (dark blue). The inset shows a stack of NSs seen from the side, evidencing their crystallinity and well-defined thickness of 2 nm. The ultrathin nanocrystals in the TEM images were colored to enhance the contrast with the background. The panels were adapted with permission from refs 24 (panel A; Copyright 2013 American Chemical Society), 34 (panel B; Copyright 2007 Royal Society of Chemistry), 35 (panel C; Copyright 2013 American Chemical Society), 39 (panel D; Copyright 2014 American Chemical Society), 25 (panel E; Copyright 2012 WILEY-VCH), 41 (panel F; Copyright 2016 American Chemical Society), 27 (panel G; Copyright 2013 Elsevier), and 40 (panel H; Copyright 2016 American Chemical Society).

nm, triangular and hexagonal, L = 100 nm −3 μm),[40] and $CsPbBr_3$ (h = 2.5 nm; square, L = 300 nm −5 μm)[41] have also been synthesized. Moreover, HgTe NPLs (h = 1.1 nm; rectangular with irregular edges, L = 100 by 300 nm) have been recently obtained by Hg^{2+} for Cd^{2+} cation exchange in template CdTe NPLs.[42] Partial topotactic Cu^+ for In^{3+} cation exchange[43] has also been recently used to convert template $Cu_{1-x}S$ NSs ($x \approx 0.03-0.07$, h = 2 nm, triangular and hexagonal, L = 150 nm) into $CuInS_2$ NSs.[44]

Colloidal NCs comprising two (or more) different semiconductors joined together by heterointerfaces offer exciting possibilities regarding property control, since the carrier localization regime in these hetero-NCs can be tailored by controlling the energy offsets between the materials that are combined.[1] In this way, hetero-NCs in the Type-I (both carriers in the same material), Type-$I^{1/2}$ (one carrier is localized in one segment of the hetero-NC, while the other probes the whole hetero-NC volume), or Type-II (spatially separated electron and hole) regimes can be obtained.[1] This strategy has been extensively used in the field of colloidal NCs,[1−10] but has only recently been extended to ultrathin 2D colloidal NCs (Figure 3), yielding Type-$I^{1/2}$ CdSe/CdS core/shell and core/crown NPLs,[23] Type-$I^{1/2}$ PbS/CdS core/shell NSs,[29] and Type-II CdSe/CdTe core/crown NPLs.[23,45] ZnSe/ZnS and PbSe/PbS core/shell NPLs have also been obtained by cation exchange reactions using CdSe/CdS core/shell NPLs as templates.[23] Ultrathin CdSe NPLs ($L \approx$ 30 by 80−140 nm) have also been encapsulated in a thin (h = 1−2 nm) amorphous silica shell, which allowed the natural helical conformation of the NPLs in solution to be preserved and fully characterized.[46] Doping is another widely employed strategy to confer novel properties to colloidal semiconductor NCs,[1] but its use in ultrathin 2D colloidal NCs is still incipient, with only a few known examples (viz., directly synthesized CdSe:Mn^{2+} NBs,[26] CdSe/CdS,Se:Mn/CdS core/multishell NPLs,[47] and CdS:Cu^+ NSs obtained by Cd^{2+} for Cu^+ cation exchange in template $Cu_{2-x}S$ NSs).[40]

Ultrathin 1D Colloidal Semiconductor Nanocrystals. The fabrication of semiconductor nanowires (NWs) by vapor phase techniques, such as metal−organic vapor phase epitaxy (MOVPE), is a very mature technology that routinely yields arrays of micrometer-long NWs on substrates with great precision over their length and diameter (>10 nm), as well as over their position and orientation relative to the substrate.[48] Solution-phase synthesis of colloidal NWs, particularly by solution−liquid−solid (SLS) epitaxy, has experienced great advances in recent years, leading to a plethora of different materials.[21] By contrast, the availability of ultrathin colloidal semiconductor NWs is still limited to just a few materials (Figure 4): Cu_2S (d = 1.7 nm, l = several μm),[49] M_2S_3 (M = Bi, Sb; d = 1.6 nm, l = 100 nm),[20] CdSe (d = 1.5 and 2.1 nm, l = several μm),[50] ZnSe (d = 1.3 nm, l = 200 nm),[51] ZnS (d = 2 nm, $l \approx$ 10 μm),[52] PbS (d = 1.8 nm, l = 200 nm),[53] $CsPbBr_3$ (d = 3.4 nm, $l \approx$ 400 nm[54] and d = 2.2 nm, $l \approx$ 100−300 nm[55]), and (Zn,Cd)Te (d = 2 nm, $l \approx$ 100 nm).[56]

Semiconductor hetero-NWs (HNWs) offer great versatility in terms of property engineering, since they can be heterostructured both radially (i.e., core/shell NWs) and axially (i.e., composition is modulated in the length direction allowing the fabrication of intra-NW p-n heterojunctions).[21,48] Nevertheless, ultrathin colloidal HNWs are even scarcer than their single-composition counterparts, and to date there is only one example reported in the literature, consisting of ∼100 nm long (Zn,Cd)Te/CdSe hetero-NWs (d = 2 nm) that are heterostructured both axially and radially (CdSe and (Zn,Cd)Te/CdSe core/shell segments follow alternately throughout the NW) (Figure 5).[56]

Formation Mechanism: Ultrathin 2D Colloidal Nanocrystals. As discussed above, ultrathin 2D colloidal NCs (NPLs, NBs, and NSs) of a variety of semiconductors have been synthesized in recent years. Their formation mechanisms, however, are still under debate, and several possibilities have been proposed (Figure 6). For example, the formation of PbS NSs (h = 2.8 nm, L ∼ 1 μm) has been ascribed by Weller and co-workers to 2D oriented attachment of PbS NCs (Figure 6).[30] The attachment is assumed to be driven by the minimization of the surface free-energy of the exposed (110) facets, followed by fusion and a

DOI: 10.1021/acs.jpclett.7b01640
J. Phys. Chem. Lett. 2017, 8, 4077−4090

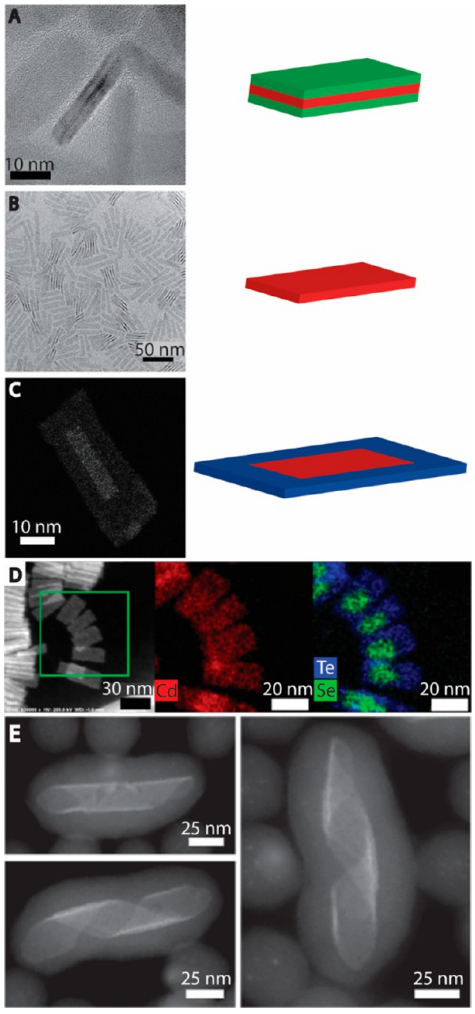

Figure 3. (A) TEM image of CdSe/CdS core/shell NPLs and a schematic representation of a core/shell NPL. The TEM image in panel B shows the CdSe NPLs used as seeds. (C) STEM image of a CdSe/CdS core/crown NPL and a schematic representation of this configuration. (D) HAADF-STEM image and elemental maps of CdSe/CdTe core/crown NPLs, clearly showing the heterointerface between the core and the crown. (E) Helical CdSe NPLs encapsulated in a thin silica shell, while preserving their helical structure. The panels were reprinted (adapted) with permission from refs 23 (panels A, B, C; Copyright 2015 American Chemical Society), 45 (panel D; Copyright 2017 American Chemical Society), and 46 (panel E; Copyright 2014 American Chemical Society).

minor reconstruction and sintering to eliminate the voids left in the intermediate "egg-tray" NC superstructure. The 2D-constraint imposed on the oriented attachment process is

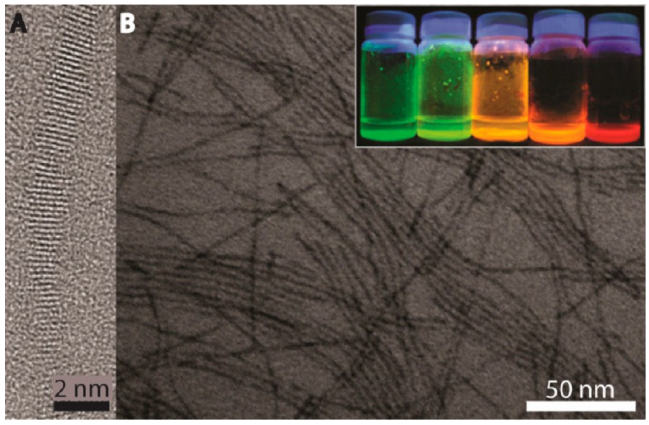

Figure 5. (A) High-resolution transmission electron microscopy image of a single colloidal (Zn,Cd)Te/CdSe hetero-NW. (B) TEM overview image of the same colloidal hetero-NW sample shown in panel A. The inset shows colloidal dispersions of (Zn,Cd)Te/CdSe hetero-NWs (2 nm diameter and ~100 nm long in all cases) with different compositions under UV illumination. The photoluminescence (PL) color can be tuned from green to red by increasing the CdSe volume fraction in the hetero-NW (PL quantum yield: 30–60%). This also results in increasingly larger electron–hole spatial separation, thereby leading to longer exciton lifetimes. Adapted with permission from ref 56. Copyright 2012 American Chemical Society.

attributed to a dense and highly ordered oleic acid layer capping the (100) facets perpendicular to the active (110) facets, which would favor the formation of extended (100) surfaces, while preventing attachment of the (100) facets.[30] 2D-oriented attachment of NC building blocks has also been suggested as a mechanism for the formation of PbSe NPLs (h = 2 nm, L ~ 50 nm) in the presence of excess chloride, which is thought to promote 2D-oriented attachment by forming inter-NC bridges.[28] In this case, the influence of the capping ligands is taken to be negligible.[28] In contrast, Buhro and co-workers proposed a mechanism for the oriented attachment of PbS NC building blocks into NSs (and NPLs) in which the ligands play a crucial role, since the 2D-constraints are assumed to be imposed by a lamellar, oleate-bilayer mesophase template.[16]

A similar mechanism, i.e., 2D-constrained self-assembly of building blocks within soft lamellar templates (Figure 6), has been invoked by both Buhro and Hyeon groups to explain the formation of wurtzite CdX (X = S, Se) NBs from Cd acetate or Cd halide precursors in long-chain (≥ C8) saturated primary alkylamine solvents at low temperatures (≤ 100 °C).[16,26] The formation of a lamellar mesophase under these conditions was confirmed by low-angle XRD.[16] The building blocks are $(CdX)_n$ magic-size clusters (MSCs), which are generated in the early stages of the reaction, as evidenced by their characteristic

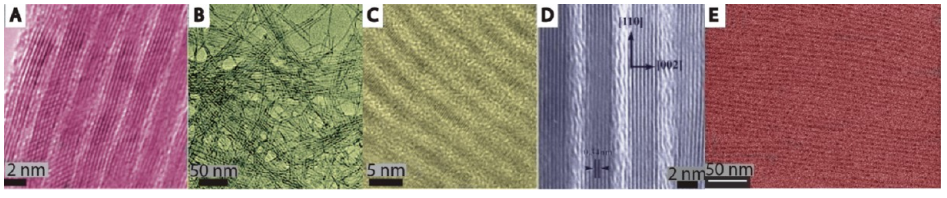

Figure 4. Examples of ultrathin colloidal nanowires: (A) PbS (pink), (B) ZnS (yellow), (C) ZnSe (yellow), (D) Cu_2S (dark blue), (E) $CsPbBr_3$ (red). The panels were adapted with permission from refs 53 (panel A; Copyright 2007 American Chemical Society), 52 (panel B; Copyright 2011 American Chemical Society), 51 (panel C; Copyright 2005 WILEY-VCH), 49 (panel D; Copyright 2005 American Chemical Society), and 55 (panel E; Copyright 2016 American Chemical Society).

DOI: 10.1021/acs.jpclett.7b01640
J. Phys. Chem. Lett. 2017, 8, 4077–4090

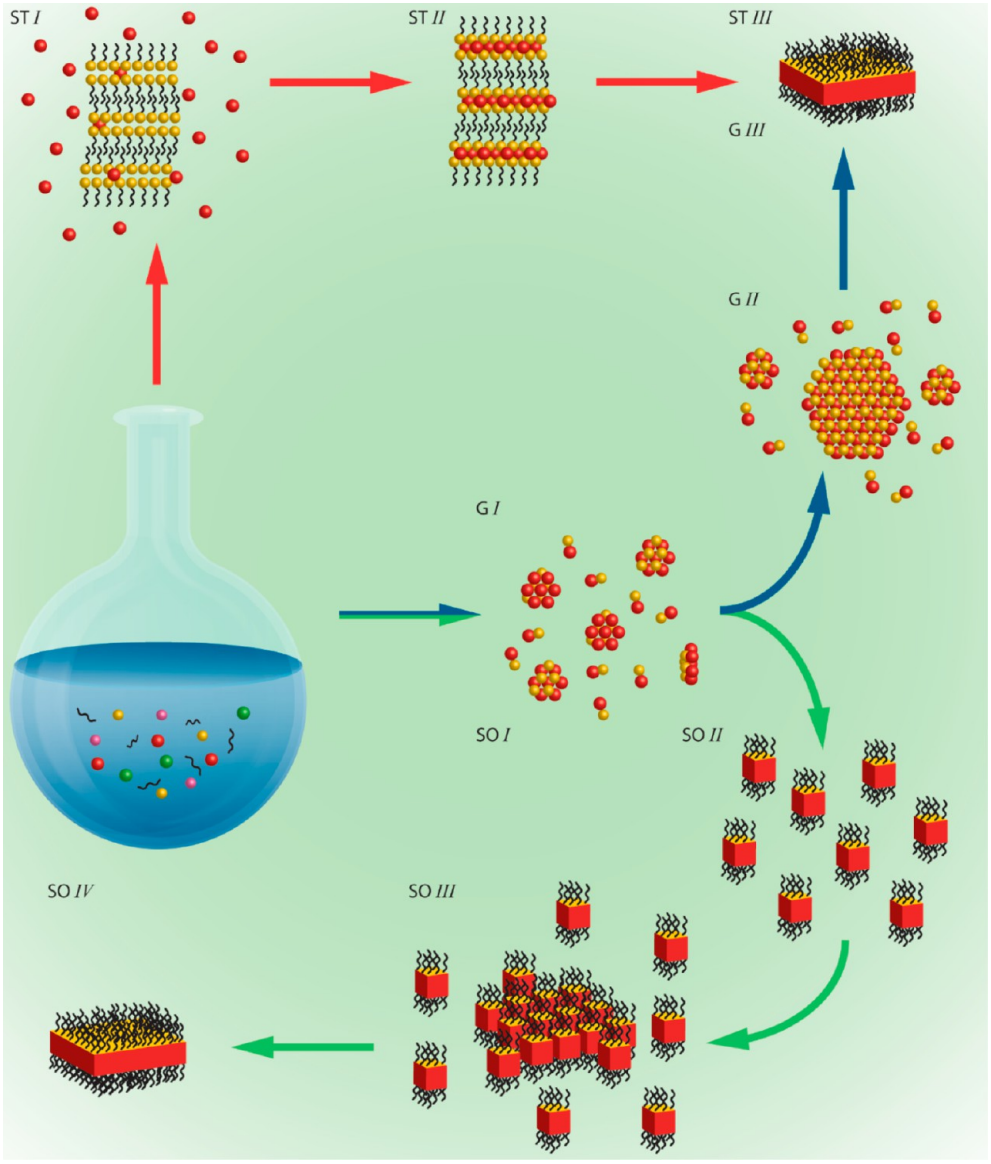

Figure 6. Schematic overview of possible formation mechanisms for ultrathin 2D NCs. The first pathway, marked with red arrows, shows the subsequent steps in the soft template (ST) mechanism, in which ligand chains order (ST *I*) and either constrain nucleation and growth in 2D, or direct the oriented attachment of building blocks in the lateral directions (ST *II*). The second pathway is marked with blue arrows and shows 2D-constrained growth (G) of magic size cluster seeds (G *I*) that grow only in lateral dimensions (G *II*) due to the directive effect of ligands (not shown for clarity) and/or facet reactivity. The last pathway, indicated by green arrows, shows NS formation through self-organization (SO). Nucleation (SO *I*) and growth of NC building blocks (SO *II*) is followed by self-organization (SO *III*) and oriented attachment (SO *IV*), directed by dense ligand layers on certain facets. After self-organizing into a 2D superstructure, the NCs fuse into a single-crystalline NS.

spectroscopic signatures (i.e., discrete and ultranarrow absorption peaks).[16,26] It is worth noting that, at reaction temperatures above 100 °C, neither ultrathin 2D NBs nor $(CdX)_n$ MSCs are obtained, but instead CdX quantum dots and nanorods form.[16,25] Moreover, CdS NBs do not form in unsaturated amines such as oleylamine, unless preformed $(CdS)_n$ MSCs are added to the reaction mixture, since they do not spontaneously form in oleylamine.[25] These observations have been taken as evidence that the formation of wurtzite CdX NBs requires reaction conditions that guarantee the stability of both soft lamellar templates and MSCs.[16,26] A soft-template mechanism has also been proposed to explain the formation of $Cu_{2-x}S$ NSs by 2D-constrained nucleation and growth within halide-stabilized lamellar Cu-thiolate complexes.[57] This mechanism was supported by *in situ* SAXS studies, which clearly demonstrated that chloride ions present in the growth medium stabilize stacks of lamellar Cu-thiolate complexes, ensuring their structural integrity beyond the onset of $Cu_{2-x}S$ nucleation.[57] Therefore, the thermolysis of the C−S bonds leads to 2D-constrained stack-templated nucleation and growth of $Cu_{2-x}S$ NSs.[57]

Interestingly, the formation of ultrathin zinc-blende CdX (X = S, Se, Te) NPLs has been explained without resorting to templating effects or oriented attachment by Dubertret and co-workers,[17,23] who proposed instead a mechanism in which the growth is due to addition of [CdX] monomers (i.e., [CdX] units formed upon reaction between Cd and X-precursors)[1] to $(CdX)_n$ MSC seeds (Figure 6).[17,23] In this mechanism, the 2D-constraints are explained by the faceting of the NPLs (the broad top and bottom surfaces are the Cd-terminated (100) facets) and the ligands used (C14−C18 long-chain carboxylic

DOI: 10.1021/acs.jpclett.7b01640
J. Phys. Chem. Lett. 2017, 8, 4077−4090

acids), which are presumed to block the top and bottom facets, thereby preventing growth in the thickness direction.[17,23] The differences with the wurtzite CdX NBs are rationalized by considering that their top and bottom surfaces consist of the nonpolar (i.e., stoichiometric) (11−20) facets.[16,23] Moreover, zinc-blende CdX NPLs are grown at higher temperatures (120−250 °C) than wurtzite CdX NBs and using stronger and less dynamic ligands (i.e., carboxylates instead of amines) diluted in a noncoordinating solvent (1-octadecene). The addition of a short-chain carboxylate (Cd acetate or propionate) to the reaction mixture appears to be critical, since, otherwise, NPLs do not form, and must occur while $(CdX)_n$ MSCs are still present.[17] Furthermore, the NPL thickness is determined by the temperature at which the short-chain carboxylate is added (higher temperatures result in thicker NPLs).[17,23]

Alternative and, to a certain extent, conflicting explanations for the formation of zinc-blende CdX NPLs have been recently proposed by both Peng and co-workers[58] and Norris and co-workers.[59] The mechanism proposed by the latter group is based on the observation that zinc-blende CdSe NPLs also form in molten Cd-carboxylates, regardless of their chain length, provided the right temperature is used (100 °C for Cd myristate, 180 °C for Cd propionate). In this model, the short-chain carboxylate is only required to make the Cd-precursor insoluble in ODE, so that the reaction can continue in phase-separated droplets of the molten salt. The 2D growth anisotropy is attributed to a much larger activation energy for island nucleation on the top and bottom large planar facets with respect to the narrow side facets, since these are smaller than the critical island size for nucleation.[59] Under the assumption that the nucleation is the rate-limiting step, this would lead to much faster growth on the thin side facets than on the large top and bottom facets. A similar argument has been proposed before by Peng and co-workers to explain the remarkable intra-NC thickness uniformity observed in 2D NCs.[60] We note that, although this model does not require selective ligand capping by long-chain carboxylic acids,[17,23] templating effects,[16] or oriented attachment,[16,28,30] it does not exclude the possibility that these processes occur, since the higher reactivity of the side facets would also be reflected in faster oriented attachment rates, while selective capping or templating effects would synergistically enhance the growth rates of the side facets. Indeed, the mechanism proposed by Peng and co-workers to explain the formation of zinc-blende CdSe 2D NCs combines the higher reactivity of the (110) side facets with selective capping and oriented attachment.[58] In contrast to the studies reported by Dubertret et al.[17,23] and Norris et al.,[59] Peng's group used preformed and purified CdSe NCs with diameter ranging from 1.7 to 2.2 nm as seeds to grow ultrathin zinc-blende CdSe NPLs (1.5 nm thick with 8 by 45 nm lateral dimensions).[58] The long hydrocarbon chains of the cadmium stearate present in the growth medium are assumed to selectively stabilize the polar (100) facets of the NCs (seeds and NPLs), leaving the reactive (110) side facets available for inter-NC 2D constrained oriented attachment.[58] The long-chain cadmium alkanoates are also thought to act as shuttles for the short-chain and insoluble cadmium acetate, bringing it to the reactive surfaces of the growing NPLs, where it promotes oriented attachment due to its very dynamic binding, which leaves the surfaces insufficiently passivated.[58]

Formation Mechanism: Ultrathin Colloidal Nanowires. A survey of the literature on ultrathin colloidal semiconductor NWs reveals that, in the majority of cases (viz., CdSe, ZnS, ZnSe, ZnTe, PbS), their formation is ascribed to oriented attachment,[50−53,56] with only two examples (viz., 1.7 nm diameter Cu_2S NWs,[49] and 1.6 nm diameter M_2S_3, M = Bi, Sb)[20] in which the 1D-anisotropic growth of the NW is attributed to selective adhesion of ligands to the side facets, thus strongly reducing their growth rate, while leaving the NW tips uncapped and therefore available for growth (Figure 7).[20,49] The selective ligand adhesion model is commonly used to explain the anisotropic growth of colloidal semiconductor nanorods and multipods,[1] and has also been used to explain the formation of ultrathin CdX NPLs (see above). However, its applicability to the growth of ultrathin NWs has yet to be unequivocally demonstrated, since the evidence presented in refs 20 and 49 in support of the proposed formation mechanism is circumstantial and has not yet been experimentally validated.

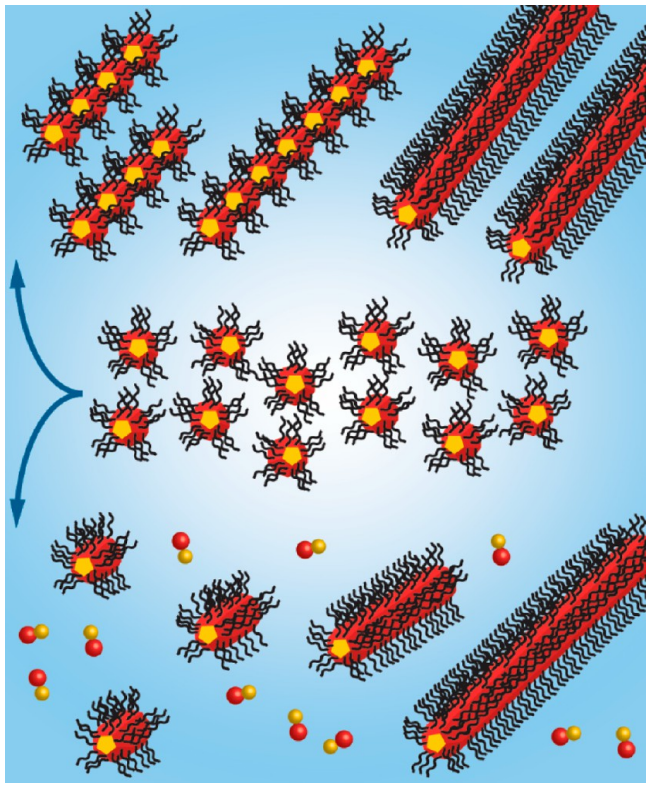

Figure 7. Schematic overview of formation mechanisms proposed for ultrathin 1D colloidal NCs. The first mechanism discussed (shown in the top of the image) is growth via self-organization of NCs or MSCs that subsequently attach and fuse. The second mechanism (shown in the lower part of the image) is growth of NCs or MSCs by monomer addition. The anisotropy of the growth is in this case attributed to selective ligand adhesion.

By contrast, the formation of ultrathin NWs by oriented attachment is supported by several pieces of evidence, of which the most significant is the observation of "pearl-necklace" aggregates at early stages of the growth.[50,52,56] These strings of interconnected particles have been observed as intermediates in the formation of colloidal wurtzite CdTe nanowires by oriented attachment of zinc-blende CdTe NCs (d = 2.5−5.6 nm), and are attributed to the first stage of the self-organization process, in which the NC building blocks are brought together by dipolar attractive interactions, thereby forming linear chain-like aggregates.[61] The presence of dipoles in NCs with the cubic zinc-blende structure is attributed to the combined effects of the shape and faceting of the NCs (truncated tetrahedra) and an

DOI: 10.1021/acs.jpclett.7b01640
J. Phys. Chem. Lett. 2017, 8, 4077−4090

asymmetric distribution of the charged ligands.[1,61] The next stage in the NW formation is reorientation to achieve proper lattice orientation, which is followed by fusion of the building blocks, recrystallization to the wurtzite phase, and sintering to eliminate inter-NC necks.[61] As a result, the diameter of the product NWs is essentially determined by the diameter of the NC building blocks. A similar mechanism has been proposed for the formation of colloidal PbSe NWs from NC building blocks (d = 4−10 nm).[1,62] Interestingly, the centrosymmetric rock-salt structure of the PbSe NC building blocks is preserved in the product NWs, since PbSe does not have an alternative anisotropic structure. Nevertheless, the oriented attachment process is also in this case assumed to be driven by dipolar interactions, which are attributed to an asymmetric distribution of anion and cation terminated facets.[1,63] It should be noted that the three stages proposed for the oriented attachment mechanism have been corroborated by an *in situ* TEM study of the coalescence of PbSe NCs into larger nanostructures.[1,64]

The centrosymmetric rock-salt structure of PbSe NC building blocks is preserved in the product NWs, since PbSe does not have an alternative anisotropic structure.

Ligands have been reported to play a decisive role in the growth of colloidal PbSe NWs by oriented attachment of PbSe NCs (d = 4−10 nm), possibly by destabilizing or selectively exposing certain facets.[1,63] For example, zigzag NWs are obtained from PbSe NCs capped by alkylamines (attachment by (111) facets), while straight NWs form when PbSe NCs capped by oleic acid are used as building blocks (attachment by (100) facets).[63] In the case of ultrathin colloidal NWs, it appears that a combination of dissimilar ligands, such as long-chain saturated primary alkylamines and acetate[50,51,56] or long-chain saturated primary alkylamines and trioctylphosphine,[52] is required, suggesting that the dipolar interactions driving the self-organization of the NC building blocks into a pearl-necklace aggregate could be the result of an asymmetric distribution of dissimilar ligands.[56] It is also possible that van der Waals interactions between the linear alkyl chains of the ligands have an adjuvant role, facilitating the self-organization into linear strings, once the NCs have been driven together by long-range dipolar interactions.[56]

Magic-Size Clusters as Synthons for Colloidal Ultrathin Low-Dimensional Nanocrystals. It is noteworthy that magic-size clusters (MSCs) have been shown to be essential for the formation of ultrathin colloidal NWs of both CdSe[50] and (Cd,Zn)Te.[56] This observation is remarkable, since $(CdX)_n$ MSCs have also been implicated in the formation of ultrathin 2D colloidal NCs (see above), both as building blocks in the 2D-templated self-assembly model proposed for wurtzite CdX NBs,[16,26] and as nuclei in the monomer addition model proposed for zinc-blende CdX NPLs.[17,23] As mentioned above, MSCs are well-defined atomically precise clusters characterized by a discrete size and a much higher stability relative to slightly smaller or larger clusters.[18,19] Consequently, growth in the magic-size regime is stepwise and quantized, going from one "magic-sized" structure to the next.[19] This offers a possible explanation for the well-defined and discrete thicknesses and diameters observed for ultrathin NCs (NWs, NPLs, NBs and NSs), since they are also in the magic-size regime. One could thus expect that the thickness or diameter of the ultrathin NCs would not only be inherited from the MSCs seeds or building blocks (for growth by monomer addition or oriented attachment, respectively), but would also be subjected to the same thermodynamic barriers that impose discrete and well-defined dimensions to MSCs. It has been demonstrated that the stability of MSCs depends critically on both the ligands used (e.g., ZnTe MSCs form with long-chain saturated primary alkylamines, but not with bulky ligands like trioctylphosphineoxide, trioctylphosphine or trioctylamine)[65] and the temperature (higher temperatures result in larger MSCs, but MSCs are no longer stable above a critical temperature).[19,65] This is consistent with the observation that the thickness of CdX NBs and NPLs increases with increasing reaction temperature.[16,17] It should be noted that the intra-NC thickness uniformity observed for colloidal NBs, NPLs, and NSs may also be rationalized by considering kinetic and thermodynamic arguments that do not require MSCs (i.e., large activation energies for 2D island nucleation on planar facets, fast 2D growth rates, and instability of kinks and ledges).[16] Moreover, it is as yet unclear whether the role of MSCs in the formation of colloidal ultrathin NCs is also significant for semiconductor families other than the II−VIs.

Correlations between Ultrathin 1D and 2D Growth. It is remarkable that the precursors and synthetic protocols used to obtain ultrathin 2D colloidal NCs are very similar to those yielding ultrathin 1D colloidal NCs. The similarity is particularly striking if one compares the synthesis methods used to prepare ultrathin wurtzite MX (M = Cd, Zn; X = Se, Te) nanowires[50,51,56] to those employed in the preparation of ultrathin wurtzite CdX (X = S, Se, Te) nanobelts (see above):[16] both involve MSCs (either preformed or formed *in situ*) and a metal acetate dispersed in molten long-chain saturated primary alkylamines. The only significant differences between the two sets of synthesis protocols are the reaction temperatures, which are typically higher for NWs than for NBs (viz., 100−180 °C and 25−100 °C, respectively). The formation mechanisms proposed for these two types of colloidal ultrathin NCs are also very similar (see above for details): 2D-constrained self-assembly of MSCs within soft lamellar templates for wurtzite CdX NBs[16,26] and oriented attachment for wurtzite MX NWs.[50,51,56] This suggests that the dimensionality (i.e., 1D or 2D) of the ultrathin product NCs formed upon oriented attachment of $(MX)_n$ MSCs is determined primarily by the reaction temperature, which must be lower than a critical limit to allow the formation of 2D NBs, since the structural integrity of the soft 2D lamellar templates is maintained by attractive van der Waals interactions between the alkyl chains of the amines. Given the short-range and weak nature of these interactions, thermal fluctuations easily disrupt the long-range in-plane order of the 2D templates, leading to a limited thermal stability. The presence of charged species introduces long-range electrostatic interactions that have a large impact on the thermal stability of the 2D template, increasing or decreasing it, depending on whether they are attractive or repulsive. For example, the addition of halides (chloride or bromide) has been shown to increase the thermal stability of 2D lamellar Cu-thiolate templates, preserving their structural integrity beyond the onset of $Cu_{2-x}S$ nucleation, thereby leading to 2D-constrained nucleation and growth of $Cu_{2-x}S$ NSs.[57] We propose that, if the electrostatic interactions are dipolar in nature, the thermally induced collapse of the 2D templates will lead to 1D templates that are likely stabilized by both dipolar

DOI: 10.1021/acs.jpclett.7b01640
J. Phys. Chem. Lett. 2017, 8, 4077−4090

interactions between the building blocks (MSCs or NCs) and van der Waals interactions between densely packed ligands organized in a tubular array in which the polar heads face inward (Figure 8). Further increase of the reaction temperature will also destabilize the 1D template and will lead to 3D growth of NCs.

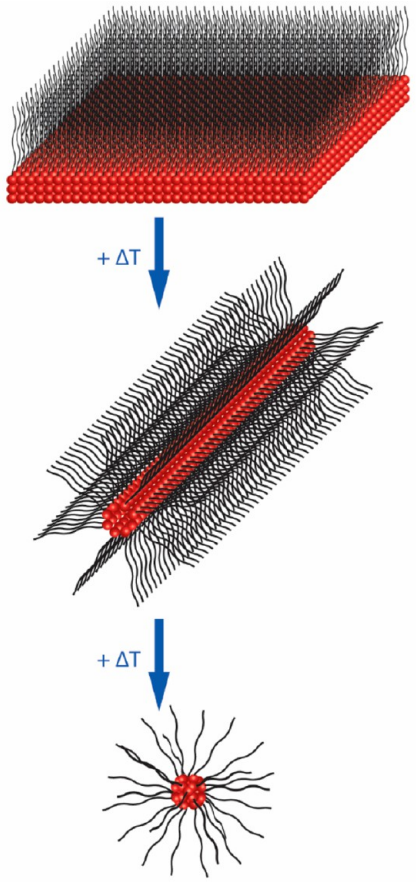

Figure 8. Top image shows a 2D NC stabilized by dense ligand layers capping the top and bottom facets (the capping layer on the bottom facet is omitted for clarity). Upon increasing temperature, the 2D ligand template collapses and forms a tubular micelle that facilitates the growth of 1D NCs, particularly in the presence of dipolar interactions between the NC or MSC building blocks. When the temperature is increased further, the micelle collapses and only 0D NCs or MSCs form.

It is as yet unclear whether the role of MSCs in the formation of colloidal ultrathin NCs is also significant for semiconductor families other than the II–VIs.

A similar model has been proposed before by Kotov and co-workers to explain the self-organization of water-soluble charge-stabilized colloidal CdTe NCs (d = 2.5–5.4 nm) into either nanowires, nanoribbons, or nanosheets, depending on the experimental conditions.[61,66,67] In their model, the authors argue that the transition from packing into chains, ribbons, or sheets can be understood in terms of a competition between face–face attraction and electrostatic repulsion.[67] For low-charge and strong short-range face attraction, the NCs pack very densely and form 2D sheets.[66] By increasing the amount of charge, an infinite sheet becomes energetically unfavorable because of the long-range electrostatic repulsion. As a result, the NCs assemble as ribbons,[67] and eventually form 1D chains upon further increase of charge.[61] The main difference between this model and the one proposed by us above is that the role of temperature is neglected by Kotov and workers, since their experiments were all carried out at a constant temperature (room temperature).[61,66,67] We thus conclude that the formation of colloidal 2D NCs is favored by strong short-range attractive potentials (typically van der Waals interactions between the ligands) and low temperatures, while 1D NCs are favored by sufficiently high temperatures, dipolar interactions, and long-range electrostatic repulsive forces. The impact of these forces will be crucial in the early stages of the formation process, in which building blocks self-organize into low-dimensional soft template superstructures (viz., lamellae or "pearl-necklace" strings for 2D or 1D NCs, respectively) that impose constraints on the NC growth, confining it to one or two dimensions. At later stages, these constraints are synergistically reinforced by short-range interactions between specific crystallographic facets of the NC (MSC) building blocks, as well as kinetic and thermodynamic driving forces for anisotropic growth that will also be active in the absence of oriented attachment and templating effects (viz., large activation energies for nucleation on large planar facets, faster growth in preferred crystallographic directions, instability of adatoms, kinks, and ledges, and selective ligand adhesion to specific facets).[1,16]

Although the discussion above was based on observations for ultrathin low-dimensional colloidal NCs of II–VI semiconductors, for which there is a wealth of experimental data, the model proposed here is likely also applicable for ultrathin NCs of other semiconductors. However, examples of materials other than II–VI semiconductors that have been obtained both as ultrathin 2D NCs and ultrathin NWs are still scarce. Among those, PbX (X = S, Se) low-dimensional NCs are probably the most extensively investigated, although typically with dimensions larger than 2 nm.[17,21,30,62,63,68] As discussed above, there are only a few examples of ultrathin low-dimensional colloidal PbX NCs (viz., PbS NWs with d = 1.8 nm,[53] PbS NSs and NBs with h = 2 nm,[29,31,69] and PbSe NPLs with h = 2 nm).[28] However, PbS NSs with $h \geq 2.8$ nm[17,30,68] and PbSe NWs with $d \geq 4$ nm[21,62,63] have been investigated in detail, and shown to form by oriented attachment of NC building blocks formed at the early stages of the reaction. These cases were already separately discussed above, in the context of the formation mechanisms of 2D and 1D colloidal NCs. Here we would like to add that, in both cases, the exact shape and faceting of the NC building blocks and the interaction of ligands with specific facets were shown to be crucial for the formation of NSs or NWs. For example, in the case of PbX NSs, reactive (110) facets attach and form necks between adjacent NCs,[28–30] possibly as a result of bridge formation by excess chlorides,[28] while attachment of the (100) facets is prevented by the presence of a dense monolayer of capping ligands (oleic acid[30] or alkylamines[28]) on those facets. By contrast, in the presence of dipolar interactions between the NCs, alkylamines will promote attachment by (111) facets, while oleic acid will induce attachment by (100) facets, yielding zigzag or straight NWs, respectively.[63] It is also important to note that the reaction temperatures for the formation of NWs (viz., 190–250 °C)[63] are significantly higher than those used to synthesize NSs (≤ 130 °C),[28–31,68] as expected based on the model discussed above.

DOI: 10.1021/acs.jpclett.7b01640
J. Phys. Chem. Lett. 2017, 8, 4077–4090

It should be noted that the first step in the formation of low-dimensional NCs is not the oriented attachment itself, but rather the self-organization of the NC building blocks into a low-dimensional templating superstructure that directs the subsequent steps. In the case of colloidal NWs, the formation of "pearl-necklace" aggregates is likely driven by the presence of sufficiently strong dipolar interactions. By contrast, as discussed above, the self-organization of NC building blocks into 2D soft template superstructures requires a more delicate balance between a number of different interactions, and may be promoted by a preexisting soft lamellar template or van der Waals interactions between the capping ligands (e.g., oleic acid molecules capping the (100) facets of colloidal PbX NCs). From this perspective, it is insightful to consider the formation of atomically coherent 2D superlattices of PbSe NCs (d = 5−6.5 nm), which have been recently studied in great detail.[70−72] In all cases, the NC superlattices were obtained by drop casting a solution of oleic acid-capped PbSe NCs on a dense, immiscible liquid surface (diethylene glycol), and allowing the solvent (toluene or hexane) to slowly evaporate at room temperature. In this method, the first step of the self-organization process is the irreversible adsorption of the NCs at the air−solvent interface, which is driven by minimization of the interfacial free energies, and is therefore affected by both the NC shape and the coverage by ligands, since some facets will adsorb more strongly than others.[73] Subsequently, as the NC concentration increases both in the solution and at the interface, the adsorbed NCs self-organize in a close-packed 2D superstructure. This process is primarily driven by maximization of the packing density, and therefore the symmetry of the resulting superlattice is largely dictated by the shape of the NC building blocks.[73]

The first step in the formation of low-dimensional NCs is not the oriented attachment itself, but rather the self-organization of the NC building blocks into a low-dimensional templating superstructure that directs the subsequent steps.

At this stage, the 2D superlattice of ligand-capped NCs is highly ordered (provided the NCs are nearly monodisperse), but not necessarily already atomically coherent. It has been recently demonstrated that the ligand coverage and the nature of the ligands may be sufficient to yield atomically aligned 2D superlattices (e.g., 2D superlattices of oleic acid capped wurtzite ZnS bifrustum-shaped NCs),[74] but this is more often driven by attractive interactions between specific facets of the NCs.[70−72] The final step is the oriented attachment itself, which requires ligand desorption from specific facets and atomic alignment, so that the equivalent facets of proximate NCs can fuse, thereby forming necks that will eventually bind all the NCs in an atomically coherent superlattice.[70−72] Depending on the exact shape and ligand coverage of the PbSe NC building blocks, and on other experimental variables that are not yet fully understood, this process will yield superlattices with either square[71,72] or buckled honeycomb[70] geometry (attachment through the (100) facets in all cases). Complete densification of the superstructure by elimination of the voids between the NCs does not happen, in contrast with the behavior observed during the formation of single crystalline colloidal PbX nanosheets by oriented attachment of colloidal PbX NCs.[28−31,68] This difference is most likely due to the significantly higher temperatures used in the latter process (100−130 °C instead of 20 °C), which promote sintering.

Properties of Ultrathin Low-Dimensional Colloidal Semiconductor Nanocrystals. Ultrathin 2D nanomaterials are attracting increasing interest due to their extraordinary electronic, optical, and mechanical properties, which make them promising materials for flexible electronics, spintronic devices, photodetectors, field-effect transistors, sensing, solar cells, batteries and supercapacitors, lasers, and LEDs.[12,13,15−17,75,76] Semiconductor nanowires are also attractive materials for a number of applications (e.g., field-effect transistors, Li-ion batteries, photocathodes for water splitting, solar cells, polarization sensitive photodetectors, thermoelectrics, etc.).[21,62] Nevertheless, as discussed above, ultrathin 1D and 2D colloidal semiconductor NCs have only recently become available, and therefore their properties have not yet been thoroughly investigated. For example, it remains to be demonstrated whether the ultrahigh carrier mobility observed in ultrathin 2D semiconductors obtained by exfoliation or MOCVD (e.g., MoS_2 and black phosphorus)[12,13,15,75,76] can also be realized in ultrathin 2D NCs prepared by solution-based "bottom-up" colloidal chemical methods. Moreover, although colloidal NCs offer the added benefit of solution processability, which has been exploited to make, e.g., field-effect transistors from colloidal PbS NSs (h = 4−20 nm)[68] and fast photodiodes from 10 nm diameter colloidal PbSe NWs,[62] the integration of ultrathin low-dimensional colloidal NCs on devices remains a challenge. This is likely due to the difficulty in removing the capping ligands and the intriguing structural features displayed by these materials (viz., ultrathin NPLs and NSs are often observed as rolled-up scrolls or stacks, while ultrathin NWs and NBs are prone to flexing, bundling, and entanglement).

In this Perspective, we will focus on the optical properties of ultrathin low-dimensional colloidal semiconductor NCs, which are of great fundamental interest because they allow the study of strongly 1D and 2D quantum confined excitons. They are also relevant from an applied viewpoint since their (potentially) narrow emission lines are very attractive for LEDs, displays, and lasers.[17,23] The most extensively investigated ultrathin colloidal NCs are CdX (X = S, Se, Te) NBs and NPLs, and, as a result, their optical properties are relatively well-understood and have been discussed in detail in a number of recent reviews.[16,17,23] Therefore, we will here only highlight the essential features of the optical properties of these materials, while attempting to establish a comparison between them and other ultrathin 1D and 2D colloidal NCs, with emphasis on materials displaying luminescence. Unfortunately, examples of the latter are scarce, which will limit our discussion to a few classes of compounds (viz., CdX,[16,17,23,56] PbX,[28−30,53,69] and $CsPbBr_3$),[32,33,54,55] for which data is available on both 1D and 2D ultrathin colloidal NCs. We will first discuss the CdX compounds, and later address the cases of PbX and $CsPbBr_3$ perovskite NCs.

The most striking feature of ultrathin colloidal CdX NPLs and NBs is their remarkably narrow absorption and photoluminescence (PL) peaks (Figure 9). For example, the full-width at half-maximum (fwhm) observed for both the lowest energy absorption feature and the PL peak of ensembles of CdSe NBs and NPLs ranges from 35 to 50 meV at room temperature.[16,17,23] These values are much narrower than

DOI: 10.1021/acs.jpclett.7b01640
J. Phys. Chem. Lett. 2017, 8, 4077−4090

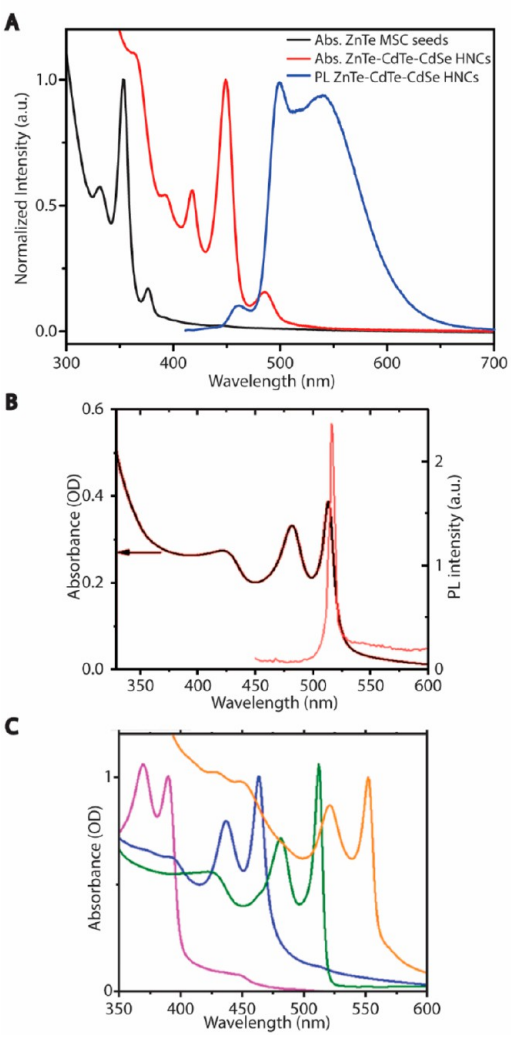

Figure 9. Absorption and PL spectra of ultrathin hetero-NWs (A) and CdSe NPLs (B). The spectra look very similar, showing sharp transitions in both absorption and PL spectra. The spectra in C are absorption spectra of CdSe NPLs of different thicknesses, which red-shift upon increasing NPL thickness. The panels were adapted with permission from refs 56 (panel A; Copyright 2012 American Chemical Society) and 17 (panels B,C; Copyright 2016 American Chemical Society).

those typically reported for QDs or nanorods, which are in the range of 80−150 meV for nearly monodisperse (size polydispersity ≤ 10%) ensembles of NCs in the 2.6−8 nm diameter range (fwhm increases for smaller d).[16,77] The fwhm for single CdSe QDs at room temperature ranges from 50 to 70 meV.[16] Moreover, the exciton confinement potential is large (0.57 E_g and 0.86 E_g for 1.8 nm thick CdSe NBs and CdTe NPLs, respectively; E_g is the bulk bandgap at 300 K, viz., 1.75 and 1.56 eV for CdSe and CdTe, respectively),[78] and increases with decreasing thickness, as evidenced by the shift of the optical transitions (Figure 9).[16,17,23] Notably, the optical transition energies of NBs and NPLs are not affected by their lateral dimensions, which shows that excitons in these NCs are strongly confined only in the thickness dimension. The ultra-narrow line widths of CdX NBs and NPLs thus implies that their optical transitions exhibit only homogeneous broadening, and therefore that intra- and inter-NC thickness variations are essentially absent.[16,17,23] This is corroborated by the observation that the fwhm is almost the same for ensemble and single CdSe NPLs.[23]

The conclusion that the NC thickness is uniform is also supported by the very small (viz., 0−30 meV) global (i.e., nonresonant) Stokes shift observed for ensembles of CdX NBs and NPLs.[16,17,23] The nonresonant Stokes shift, $\Delta_{ST}(nr)$, is the energy difference between the lowest-energy absorption peak and the PL peak of an ensemble of NCs, and has been reported to range from 20 to100 meV for CdSe QDs in the 9−2.2 nm diameter range, and 35−100 meV for CdSe nanorods ($d \approx 3-5$ nm, aspect ratio = 2−10).[16,77] The apparent size dependence of the $\Delta_{ST}(nr)$ values has been attributed to the combined effects of the exciton fine-structure and the inhomogeneous size distribution.[77] The impact of the ensemble size distribution on the observed $\Delta_{ST}(nr)$ values is due to the fact that the absorption cross sections of QDs and nanorods at energies far above the band-edge scale with the volume.[78] Therefore, larger NCs will absorb relatively more light upon excitation at energies above the band edge, resulting in a redshift of the ensemble PL spectrum from the statistically weighted maximum. The observation of small $\Delta_{ST}(nr)$ for ensembles of CdX NBs and NPLs is thus consistent with a negligible thickness distribution.[16]

The sharp peaks observed in the absorption spectra of CdX NPLs and NBs have been ascribed to quantum-well transitions, with the first two exciton resonances being assigned to the $1_{hh} - 1_e$ and $1_{lh} - 1_e$ transitions, respectively (hh = heavy-hole, lh = light-hole, e = electron).[16,23,79] The carrier confinement in colloidal NBs and NPLs is, however, stronger than in epitaxial quantum wells, since the former are surrounded by a low dielectric constant medium (organic solvents or air), while the latter are embedded in a crystal of a different semiconductor.[23,79] This results in larger exciton binding energies and, consequently, enhanced oscillator strengths, which are reflected in shorter exciton radiative lifetimes (a few ns at room temperature and 150−300 ps at 4 K).[17,79]

Ultra-narrow features have also been observed in the absorption spectra of ultrathin colloidal wurtzite (Zn,Cd)Te and (Zn,Cd)Te/CdSe NWs (Figure 9).[56] The fwhm of these features (viz., 95 meV)[56] is even narrower than that of the ZnTe MSCs (viz., 150 meV)[56,65] from which they formed by partial cation exchange followed by oriented attachment (see above and ref 56 for details). This implies that intra- and inter-NW diameter variations are very small. However, a detailed comparison of the optical properties of these NWs to those of the CdX NPLs and NBs discussed above is complicated by the heterostructured nature of the NWs, which consist of segments that are heterostructured on a length scale of the order of 2−10 nm.[56] This is particularly evident in the PL spectra and in the exciton lifetimes, and will be discussed in more detail below, in conjunction with the optical properties of CdX-based hetero-NPLs. Future efforts should thus be directed toward developing single composition colloidal ultrathin CdX NWs, which would allow a direct comparison between ultrathin CdX NWs, NPLs and NBs. A study by Loomis and co-workers has shown that photogenerated electron−hole pairs in 7 nm diameter colloidal CdSe NWs are bound as 1D excitons at room temperature.[80] It may thus be expected that the exciton decay and the optical properties of the ultrathin colloidal (Zn,Cd)Te and (Zn,Cd)Te/CdSe NWs reported in ref 56 were also dominated by strongly bound 1D excitons. Ultrathin colloidal NWs of wurtzite ZnSe and ZnS have also been reported,[51,52] but their luminescence was dominated by defect-assisted recombination, leading to very

DOI: 10.1021/acs.jpclett.7b01640
J. Phys. Chem. Lett. 2017, 8, 4077−4090

broad PL peaks (fwhm: ~ 500−600 meV), despite sharp lowest energy absorption peaks (fwhm: ~ 200 meV).

The PL quantum yields (QYs) of organically passivated CdSe NPLs and NBs are remarkably high (viz., 20−30%) considering their large surface to volume ratio, and can reach values as high as 80% for CdSe/CdS core/shell NPLs.[16,17,23] These values are comparable to those reported for QDs and quantum rods and ~1−2 orders of magnitude higher than those typically reported for nanowires (< 1%).[16,21] The high PLQYs of bare CdSe NPLs and NBs imply that the top and bottom facets are very well passivated by ligands.[16] However, the impact of the large surface/volume ratio of the NBs and NPLs on their PLQYs is still noticeable, since the PLQYs of organically capped colloidal CdSe QDs can reach values as high as 85%.[1] It should be noted that CdX-based NWs with reasonably high PLQYs are uncommon, but have nevertheless been reported (viz., 7 nm diameter CdTe/CdS core/shell NW with PLQY = 25%[21] and thioglycolic acid-stabilized CdTe NWs with PLQY = 29% for d = 2.5 nm and 2.3% for d = 5.6 nm).[61] In this context, the PLQYs of the ultrathin (d = 2 nm) colloidal (Zn,Cd)Te and (Zn,Cd)Te/CdSe hetero-NWs studied by Groeneveld and co-workers (viz., 20−60%)[56] (Figure 5) are exceptional, and may be attributed to a combination of the heterostructured nature of the NWs and a very efficient surface passivation by hexadecylamine ligands.

Ultrathin colloidal CdSe-based heterostructured NPLs have also been studied in detail.[17,23] Overcoating CdSe NPLs with CdS layers, thereby forming Type-I$^{1/2}$ CdSe/CdS core/shell NPLs, has been observed to greatly improve the PLQYs (up to 80%), while shifting both the absorption and the PL spectra to lower energies by ~360 meV and increasing the fwhm of the PL peak from 37 to 65 meV.[17,23] The red-shift of the optical transitions can be ascribed to relaxation of the quantum confinement due to delocalization of the electron wave function over the entire NPL thickness, while the increase in the fwhm likely reflects a distribution in the CdS shell thickness within the NPL ensemble. Spectral red-shifts have also been observed upon exchange of the native ligands (n-octylamine) on wurtzite CdSe NBs by Cd(oleate)$_2$ (140 ± 20 meV shift) or Zn(oleate)$_2$ (30 ± 20 meV shift),[81] or upon encapsulation of zinc-blende CdSe NPLs in a thin silica shell (130−160 meV shift).[46] These shifts have been attributed entirely to strain for exchange with Zn(oleate)$_2$,[81] and to a combination of strain and extension of the confinement dimension for exchange with Cd(oleate)$_2$ or SiO$_2$ encapsulation.[46,81]

By contrast, extension of the lateral dimensions of CdSe NPLs with CdS, thereby forming Type-I$^{1/2}$ CdSe/CdS core/crown NPLs, does not induce any significant spectral shift, consistent with the fact that there is essentially no quantum confinement in the lateral dimensions of NBs and NPLs.[17,23] However, the PLQYs increase to values as high as 60%, demonstrating that unpassivated sites on the lateral facets are efficient quenching centers. Interestingly, pronounced spectral shifts are observed for Type-II CdSe/CdTe core/crown NPLs, which exhibit PL at much longer wavelengths than those of the seed CdSe NPLs (viz., 650 nm instead of 510 nm).[17] The absorption peaks remain narrow, but the fwhm of the PL peak and the $\Delta_{ST}(nr)$ value increase to 170 and 300 meV, respectively, while the exciton lifetimes become longer (200−300 ns).[17] These changes can be attributed to the spatial separation of the electron and hole in, respectively, the CdSe core and the CdTe crown, leading to the formation of a spatially indirect exciton.[1] Similar spectral features have been reported for ultrathin colloidal (Zn,Cd)Te/CdSe hetero-NWs (Figure 9), in which the hole and electron wave functions localize primarily in the (Zn,Cd)Te and CdSe segments of the hetero-NW, respectively.[56] As a result, the overlap between the electron and hole wave functions in these hetero-NWs can be tailored by controlling the CdSe volume fraction, allowing the PL wavelength to be tuned from 530 to 760 nm, with a concomitant increase in the exciton lifetimes from 20 to 700 ns.[56] Interestingly, for sufficiently small CdSe volume fractions, direct and spatially indirect 1D excitons coexist in the hetero-NW, leading to both narrow PL peaks with negligible $\Delta_{ST}(nr)$ and broad PL peaks with large $\Delta_{ST}(nr)$ (Figure 9).[56]

The optical properties of ultrathin 1D and 2D colloidal NCs of PbX (X = S, Se) and CsPbBr$_3$ perovskites have also been investigated, albeit to a limited extent. Intriguingly, the absorption spectra of ultrathin PbX NWs, NBs, NPLs, and NSs do not show any discernible features,[28−30,53,69] in striking contrast not only with the absorption spectra of ultrathin colloidal CdX NCs (see above), but also with the well-defined features typically observed in the absorption spectra of ensembles of colloidal PbX QDs.[82] The PL peaks are also typically broader (fwhm: ~ 200−250 meV)[28−30,53] than those observed for ultrathin CdX NCs, although remarkably narrow PL peaks (fwhm ~100−150 meV) have been recently reported by Khan et al. for PbS NPLs prepared from a single-source precursor.[69] These observations have been interpreted as evidence that the thickness of PbX NBs, NPLs, and NSs is often not atomically uniform, both over a single NC and across the ensemble.[29] The reported PLQYs are very low (viz., 0.1−6%),[28,29] implying that the surface passivation of ultrathin colloidal PbX NCs is much less efficient than that achieved for the CdX analogues discussed above. Owing to the large exciton Bohr radii of PbX compounds (a_0 = 20 and 46 nm for X = S and Se, respectively),[82] the confinement potential experienced by excitons in ultrathin colloidal PbX NCs is extremely large, reaching values as high as ~3 E_g for ~2 nm thick PbX NSs and NPLs[28−30] and ~6 E_g for 1.8 nm diameter PbS NWs.[53] These materials thus offer unique opportunities for studying the properties of excitons in extreme quantum confinement, since the ratio between the size of NCs in the ultrathin regime and the exciton Bohr radius is very small (viz., $d/2a_0 \leq 0.1$ and 0.04 for PbS and PbSe, respectively, and ≤ 0.4 and 0.27 for CdSe and CdTe, respectively).

Colloidal CsPbX$_3$ (X = Cl, Br, I) perovskite NCs are attracting huge interest from the scientific community due to their outstanding optical properties (viz., narrow PL tunable throughout the entire visible spectrum with QYs up to 90%), which make them promising materials for various optoelectronic applications, such as low threshold lasers, highly efficient LEDs, and solution processed solar cells.[83−88] This intense research activity has resulted in synthetic protocols for colloidal CsPbX$_3$ NCs with a variety of shapes, such as cubes, nanowires, nanoplatelets, and, since recently, also ultrathin NWs and NSs.[32,33,54,55] As expected, quantum confinement effects are more pronounced in the ultrathin NCs, but are nevertheless relatively small if compared to those observed for the CdX and PbX analogues (confinement potential is only ~0.5 eV or 0.2 E_g for CsPbBr$_3$ NWs and NSs). These relatively modest confinement potentials reflect the fact that the exciton Bohr radius of CsPbBr$_3$ (3.5 nm)[83] is smaller than those of CdX (4.9 and 7.3 nm for X = Se and Te, respectively)[78] and PbX (20 and 46 nm for X = S and Se, respectively).[82] The bandwidth of the optical transitions increases slightly upon size reduction to the ultrathin regime, viz., from 80 meV[83,88] to ~80−170 meV (depending on the sample),[32,33,54,55] while the PLQYs decrease to ~10−30%.

DOI: 10.1021/acs.jpclett.7b01640
J. Phys. Chem. Lett. 2017, 8, 4077−4090

The lower PLQYs are likely due to the increase in the surface area of the NCs, associated with poorer surface passivation, but may also reflect the fact that orthorhombic domains coexist with the cubic perovskite phase in ultrathin colloidal $CsPbBr_3$ NSs,[89] since the PLQYs of the orthorhombic phase are known to be lower than those of the cubic phase.[83] Moreover, the stability of ultrathin colloidal $CsPbBr_3$ NWs and NSs is also lower than that of larger $CsPbBr_3$ NCs.[32,33,55]

In summary, research on ultrathin nanomaterials has become one of the fastest developing areas in contemporary nanoscience, and is posed to play a crucial role in the development of novel and disruptive technologies. The field of ultrathin colloidal semiconductor NCs is still in its infancy, and requires a lot more work to reach the level of maturity already achieved by other synthetic methods such as, e.g., exfoliation or chemical vapor deposition. The most attractive prospect of colloidal chemical methods is that they may enable the realization of high-yield and high-throughput production of free-standing ultrathin 1D and 2D NCs of nonlayered materials in liquid-phase at relatively low costs, and with versatility in terms of composition, size, shape, and surface control. However, most research to date has been focused on the prototypical Cd-chalcogenides, with particular emphasis on 2D and quasi-2D NCs. Future research should thus be directed toward exploring novel compositions, such as multinary chalcogenides (e.g., $CuInS_2$ and Cu_2ZnSnS_4) or transition metal chalcogenides (e.g., MoS_2), and further developing materials that are just beginning to emerge as ultrathin colloidal NCs, such as lead, copper, and indium chalcogenides. The synthesis of colloidal ultrathin NWs is particularly underdeveloped, and therefore requires significant efforts to reach an adequate level of control. Finally, as discussed above, the formation mechanisms of ultrathin 2D and 1D colloidal NCs are still under debate, even for the prototypical CdX NPLs and NBs, and should thus be investigated in more detail using *in situ* techniques, such as *in situ* transmission electron microscopy, powder X-ray diffraction, and small-angle X-ray scattering.

Research on ultrathin nanomaterials has become one of the fastest developing areas in contemporary Nanoscience, and is posed to play a crucial role in the development of novel and disruptive technologies.

AUTHOR INFORMATION

Corresponding Author

*E-mail: c.demello-donega@uu.nl.

ORCID

Celso de Mello Donega: 0000-0002-4403-3627

Notes

The authors declare no competing financial interest.

Biographies

Anne C. Berends received her M.Sc. in Chemistry from Utrecht University in 2014. She is currently a Ph.D. candidate in the Debye Institute for Nanomaterials Science of the same university, investigating the synthesis and optical properties of colloidal nanocrystals of ternary $I-III-VI_2$ copper chalcogenides.

Dr. Celso de Mello Donega is an Associate Professor in the Chemistry Department of the Faculty of Sciences at Utrecht University in The Netherlands. He earned his Ph.D. degree in Chemistry from Utrecht University in 1994. His research is focused on the chemistry and optoelectronic properties of nanomaterials, with particular emphasis on colloidal nanocrystals and heteronanocrystals of semiconductors.

ACKNOWLEDGMENTS

The authors acknowledge financial support from the division of Chemical Sciences (CW) of The Netherlands Organization for Scientific Research (NWO) under grant number ECHO.712.014.001.

REFERENCES

(1) Donega, C. d. M. Synthesis and Properties of Colloidal Heteronanocrystals. *Chem. Soc. Rev.* **2011**, *40*, 1512−1546.
(2) Kovalenko, M. V.; Manna, L.; Cabot, A.; Hens, Z.; Talapin, D. V.; Kagan, C. R.; Klimov, V. I.; Rogach, A. L.; Reiss, P.; Milliron, D. J.; et al. Prospects of Nanoscience with Nanocrystals. *ACS Nano* **2015**, *9*, 1012−1057.
(3) Grim, J. Q.; Manna, L.; Moreels, I. A. Sustainable Future for Photonic Colloidal Nanocrystals. *Chem. Soc. Rev.* **2015**, *44*, 5897−5914.
(4) Reiss, P.; Carrière, M.; Lincheneau, C.; Vaure, L.; Tamang, S. Synthesis of Semiconductor Nanocrystals, Focusing on Nontoxic and Earth-Abundant Materials. *Chem. Rev.* **2016**, *116*, 10731−10819.
(5) Jing, L.; Kershaw, S. V.; Li, Y.; Huang, X.; Li, Y.; Rogach, A. L.; Gao, M. Aqueous Based Semiconductor Nanocrystals. *Chem. Rev.* **2016**, *116*, 10623−10730.
(6) van der Stam, W.; Berends, A. C.; de Mello Donega, C. Prospects of Colloidal Copper Chalcogenide Nanocrystals. *ChemPhysChem* **2016**, *17*, 559−581.
(7) De Trizio, L.; Manna, L. Forging Colloidal Nanostructures via Cation Exchange Reactions. *Chem. Rev.* **2016**, *116*, 10852−10887.
(8) Boles, M. A.; Engel, M.; Talapin, D. V. Self-Assembly of Colloidal Nanocrystals: From Intricate Structures to Functional Materials. *Chem. Rev.* **2016**, *116*, 11220−11289.
(9) Pietryga, J. M.; Park, Y.-S.; Lim, J.; Fidler, A. F.; Bae, W. K.; Brovelli, S.; Klimov, V. I. Spectroscopic and Device Aspects of Nanocrystal Quantum Dots. *Chem. Rev.* **2016**, *116*, 10513−10622.
(10) Rabouw, F. T.; de Mello Donega, C. Excited-State Dynamics in Colloidal Semiconductor Nanocrystals. *Top Curr. Chem. (Z)* **2016**, *374*, 58.
(11) Novoselov, K. S.; Geim, A. K.; Morozov, S. V.; Jiang, D.; Zhang, Y.; Dubonos, S. V.; Grigorieva, I. V.; Firsov, A. A. Electric Field Effect in Atomically Thin Carbon Films. *Science* **2004**, *306*, 666−669.
(12) Butler, S. Z.; Hollen, S. M.; Cao, L.; Cui, Y.; Gupta, J. A.; Gutierrez, H. R.; Heinz, T. F.; Hong, S. S.; Huang, J.; Ismach, A. F.; et al. Progress, Challenges, and Opportunities in Two-Dimensional Materials Beyond Graphene. *ACS Nano* **2013**, *7*, 2898−2926.
(13) Xu, M.; Liang, T.; Shi, M.; Chen, H. Graphene-Like Two-Dimensional Materials. *Chem. Rev.* **2013**, *113*, 3766−3798.
(14) Heine, T. Transition Metal Chalcogenides: Ultrathin Inorganic Materials with Tunable Electronic Properties. *Acc. Chem. Res.* **2015**, *48*, 65−72.
(15) Zhang, H. Ultrathin Two-Dimensional Nanomaterials. *ACS Nano* **2015**, *9*, 9451−9469.
(16) Wang, F.; Wang, Y.; Liu, Y.-H.; Morrison, P. J.; Loomis, R. A.; Buhro, W. E. Two-Dimensional Semiconductor Nanocrystals: Properties, Templated Formation, and Magic-Size Nanocluster Intermediates. *Acc. Chem. Res.* **2015**, *48*, 13−21.
(17) Nasilowski, M.; Mahler, B.; Lhuillier, E.; Ithurria, S.; Dubertret, B. Two-Dimensional Colloidal Nanocrystals. *Chem. Rev.* **2016**, *116*, 10934−10982.

DOI: 10.1021/acs.jpclett.7b01640
J. Phys. Chem. Lett. 2017, 8, 4077−4090

(18) Jin, R.; Zeng, C.; Zhou, M.; Chen, Y. Atomically Precise Colloidal Metal Nanoclusters and Nanoparticles: Fundamentals and Opportunities. *Chem. Rev.* **2016**, *116*, 10346−10413.
(19) Friedfeld, M. R.; Stein, J. L.; Cossairt, B. M. Main-Group-Semiconductor Cluster Molecules as Synthetic Intermediates to Nanostructures. *Inorg. Chem.* **2017**, *56*, 8689.
(20) Cademartiri, L.; Ozin, G. A. Ultrathin Nanowires − A Materials Chemistry Perspective. *Adv. Mater.* **2009**, *21*, 1013−1020.
(21) Wang, F.; Dong, A.; Buhro, W. E. Solution−Liquid−Solid Synthesis, Properties, and Applications of One-Dimensional Colloidal Semiconductor Nanorods and Nanowires. *Chem. Rev.* **2016**, *116*, 10888−10933.
(22) Bouet, C.; Tessier, M. D.; Ithurria, S.; Mahler, B.; Nadal, B.; Dubertret, B. Flat Colloidal Semiconductor Nanoplatelets. *Chem. Mater.* **2013**, *25*, 1262−1271.
(23) Lhuillier, E.; Pedetti, S.; Ithurria, S.; Nadal, B.; Heuclin, H.; Dubertret, B. Two-Dimensional Colloidal Metal Chalcogenides Semiconductors: Synthesis, Spectroscopy, and Applications. *Acc. Chem. Res.* **2015**, *48*, 22−30.
(24) Bouet, C.; Mahler, B.; Nadal, B.; Abecassis, B.; Tessier, M. D.; Ithurria, S.; Xu, X.; Dubertret, B. Two-Dimensional Growth of CdSe Nanocrystals, from Nanoplatelets to Nanosheets. *Chem. Mater.* **2013**, *25*, 639−645.
(25) Son, J. S.; Park, K.; Kwon, S. G.; Yang, J.; Choi, M. K.; Kim, J.; Yu, J. H.; Joo, J.; Hyeon, T. Dimension-Controlled Synthesis of CdS Nanocrystals: From 0D Quantum Dots to 2D Nanoplates. *Small* **2012**, *8*, 2394−2402.
(26) Yang, J.; Son, J. S.; Yu, J. H.; Joo, J.; Hyeon, T. Advances in the Colloidal Synthesis of Two-Dimensional Semiconductor Nanoribbons. *Chem. Mater.* **2013**, *25*, 1190−1198.
(27) Park, H.; Chung, H.; Kim, W. Synthesis of Ultrathin Wurtzite ZnSe Nanosheets. *Mater. Lett.* **2013**, *99*, 172−175.
(28) Koh, W.-K.; Dandu, N. K.; Fidler, A. F.; Klimov, V. I.; Pietryga, J. M.; Kilina, S. V. Thickness-Controlled Quasi-Two-Dimensional Colloidal PbSe Nanoplatelets. *J. Am. Chem. Soc.* **2017**, *139*, 2152−2155.
(29) Zhang, H.; Savitzky, B. H.; Yang, J.; Newman, J. T.; Perez, K. A.; Hyun, B.-R.; Kourkoutis, L. F.; Hanrath, T.; Wise, F. W. Colloidal Synthesis of PbS and PbS/CdS Nanosheets Using Acetate-Free Precursors. *Chem. Mater.* **2016**, *28*, 127−134.
(30) Schliehe, C.; Juarez, B. H.; Pelletier, M.; Jander, S.; Greshnykh, D.; Nagel, M.; Meyer, A.; Foerster, S.; Kornowski, A.; Klinke, C.; Weller, H. Ultrathin PbS Sheets by Two-Dimensional Oriented Attachment. *Science* **2010**, *329*, 550−553.
(31) Khan, A. H.; Pal, S.; Dalui, A.; Pradhan, J.; Sarma, D. D.; Acharya, S. Solution-Processed Free-Standing Ultrathin Two-Dimensional PbS Nanocrystals with Efficient and Highly Stable Dielectric Properties. *Chem. Mater.* **2017**, *29*, 1175−1182.
(32) Akkerman, Q. A.; Motti, S. G.; Srimath Kandada, A. R.; Mosconi, E.; D'Innocenzo, V.; Bertoni, G.; Marras, S.; Kamino, B. A.; Miranda, L.; De Angelis, F.; et al. Solution Synthesis Approach to Colloidal Cesium Lead Halide Perovskite Nanoplatelets with Monolayer-Level Thickness Control. *J. Am. Chem. Soc.* **2016**, *138*, 1010−1016.
(33) Bekenstein, Y.; Koscher, B. A.; Eaton, S. W.; Yang, P.; Alivisatos, A. P. Highly Luminescent Colloidal Nanoplates of Perovskite Cesium Lead Halide and Their Oriented Assemblies. *J. Am. Chem. Soc.* **2015**, *137*, 16008−16011.
(34) Malakooti, R.; Cademartiri, L.; Migliori, A.; Ozin, G. A. Ultrathin Sb_2S_3 Nanowires and Nanoplatelets. *J. Mater. Chem.* **2008**, *18*, 66−69.
(35) Li, L.; Chen, Z.; Hu, Y.; Wang, X.; Zhang, T.; Chen, W.; Wang, Q. Single-Layer Single-Crystalline SnSe Nanosheets. *J. Am. Chem. Soc.* **2013**, *135*, 1213−1216.
(36) Acharya, S.; Sarkar, S.; Pradhan, N. Subnanometer Thin β-Indium Sulfide Nanosheets. *J. Phys. Chem. Lett.* **2012**, *3*, 3812−3817.
(37) Almeida, G.; Dogan, S.; Bertoni, G.; Giannini, C.; Gaspari, R.; Perissinotto, S.; Krahne, R.; Ghosh, S.; Manna, L. Colloidal Monolayer β-In_2Se_3 Nanosheets with High Photoresponsivity. *J. Am. Chem. Soc.* **2017**, *139*, 3005−3011.
(38) Lauth, J.; Gorris, F. E. S.; Samadi Khoshkhoo, M.; Chassé, T.; Friedrich, W.; Lebedeva, V.; Meyer, A.; Klinke, C.; Kornowski, A.; Scheele, M.; et al. Solution-Processed Two-Dimensional Ultrathin InSe Nanosheets. *Chem. Mater.* **2016**, *28*, 1728−1736.
(39) Mahler, B.; Hoepfner, V.; Liao, K.; Ozin, G. Colloidal Synthesis of 1T-WS_2 and 2H-WS_2 Nanosheets: Applications for Photocatalytic Hydrogen Evolution. *J. Am. Chem. Soc.* **2014**, *136*, 14121−14127.
(40) van der Stam, W.; Akkerman, Q. A.; Ke, X.; van Huis, M. A.; Bals, S.; de Mello Donega, C. Solution-Processable Ultrathin Size- and Shape-Controlled Colloidal $Cu_{2-x}S$ Nanosheets. *Chem. Mater.* **2015**, *27*, 283−291.
(41) Shamsi, J.; Dang, Z.; Bianchini, P.; Canale, C.; Di Stasio, F.; Brescia, R.; Prato, M.; Manna, L. Colloidal Synthesis of Quantum Confined Single Crystal $CsPbBr_3$ Nanosheets with Lateral Size Control up to the Micrometer Range. *J. Am. Chem. Soc.* **2016**, *138*, 7240−7243.
(42) Izquierdo, E.; Robin, A.; Keuleyan, S.; Lequeux, N.; Lhuillier, E.; Ithurria, S. Strongly Confined HgTe 2D Nanoplatelets as Narrow Near-Infrared Emitters. *J. Am. Chem. Soc.* **2016**, *138*, 10496−10501.
(43) van der Stam, W.; Berends, A. C.; Rabouw, F. T.; Willhammar, T.; Ke, X.; Meeldijk, J. D.; Bals, S.; de Mello Donega, C. Luminescent $CuInS_2$ Quantum Dots by Partial Cation Exchange in $Cu_{2-X}S$ Nanocrystals. *Chem. Mater.* **2015**, *27*, 621−628.
(44) Mu, L.; Wang, F.; Buhro, W. E. Exciton Splitting in Thin Copper Indium Disulfide Nanosheets. *Chem. Mater.* **2017**, *29*, 3686−3693.
(45) Li, Q.; Xu, Z.; McBride, J. R.; Lian, T. Low Threshold Multiexciton Optical Gain in Colloidal CdSe/CdTe Core/Crown Type-II Nanoplatelet Heterostructures. *ACS Nano* **2017**, *11*, 2545−2553.
(46) Hutter, E. M.; Bladt, E.; Goris, B.; Pietra, F.; van der Bok, J. C.; Boneschanscher, M. P.; de Mello Donega, C.; Bals, S.; Vanmaekelbergh, D. Conformal and atomic characterization of ultrathin CdSe platelets with a helical shape. *Nano Lett.* **2014**, *14*, 6257−6262.
(47) Delikanli, S.; Akgul, M. Z.; Murphy, J. R.; Barman, B.; Tsai, Y.; Scrace, T.; Zhang, P.; Bozok, B.; Hernández-Martínez, P. L.; Christodoulides, J.; et al. Mn^{2+}-Doped CdSe/CdS Core/Multishell Colloidal Quantum Wells Enabling Tunable Carrier-Dopant Exchange Interactions. *ACS Nano* **2015**, *9*, 12473−12479.
(48) Dasgupta, N. P.; Sun, J.; Liu, C.; Brittman, S.; Andrews, S. C.; Lim, J.; Gao, H.; Yan, R.; Yang, P. Semiconductor Nanowires − Synthesis, Characterization, and Applications. *Adv. Mater.* **2014**, *26*, 2137−2184.
(49) Liu, Z. P.; Xu, D.; Liang, J. B.; Shen, J. M.; Zhang, S. Y.; Qian, Y. T. Growth of Cu_2S Ultrathin Nanowires in a Binary Surfactant Solvent. *J. Phys. Chem. B* **2005**, *109*, 10699−10704.
(50) Pradhan, N.; Xu, H. F.; Peng, X. G. Colloidal CdSe Quantum Wires by Oriented Attachment. *Nano Lett.* **2006**, *6*, 720−724.
(51) Panda, A. B.; Acharya, S.; Efrima, A. Ultranarrow ZnSe Nanorods and Nanowires: Structure, Spectroscopy, and One-Dimensional Properties. *Adv. Mater.* **2005**, *17*, 2471−2474.
(52) Zhu, G.; Zhang, S.; Xu, Z.; Ma, J.; Shen, X. Ultrathin ZnS Single Crystal Nanowires: Controlled Synthesis and Room-Temperature Ferromagnetism Properties. *J. Am. Chem. Soc.* **2011**, *133*, 15605−15612.
(53) Patla, I.; Acharya, S.; Zeiri, L.; Israelachvili, J.; Efrima, S.; Golan, Y. Synthesis, Two-Dimensional Assembly, and Surface Pressure-Induced Coalescence of Ultranarrow PbS Nanowires. *Nano Lett.* **2007**, *7*, 1459−1462.
(54) Imran, M.; Di Stasio, F.; Dang, Z.; Canale, C.; Khan, A. H.; Shamsi, J.; Brescia, R.; Prato, M.; Manna, L. Colloidal Synthesis of Strongly Fluorescent $CsPbBr_3$ Nanowires with Width Tunable down to the Quantum Confinement Regime. *Chem. Mater.* **2016**, *28*, 6450−6454.
(55) Zhang, D.; Yu, Y.; Bekenstein, Y.; Wong, A. B.; Alivisatos, A. P.; Yang, P. Ultrathin Colloidal Cesium Lead Halide Perovskite Nanowires. *J. Am. Chem. Soc.* **2016**, *138*, 13155−13158.
(56) Groeneveld, E.; van Berkum, S.; van Schooneveld, M. M.; Gloter, A.; Meeldijk, J. D.; van den Heuvel, D. J.; Gerritsen, H. C.; de Mello Donegá, C. Highly Luminescent (Zn,Cd)Te-CdSe Colloidal Heteronanowires with Tunable Electron-Hole Overlap. *Nano Lett.* **2012**, *12*, 749−757.
(57) van der Stam, W.; Rabouw, F. T.; Geuchies, J. J.; Berends, A. C.; Hinterding, S. O. M.; Geitenbeek, R. G.; van der Lit, J.; Prévost, S.; Petukhov, A. V.; de Mello Donega, C. *In Situ* Probing of Stack-

DOI: 10.1021/acs.jpclett.7b01640
J. Phys. Chem. Lett. 2017, 8, 4077−4090

Templated Growth of Ultrathin $Cu_{2-x}S$ Nanosheets. *Chem. Mater.* **2016**, *28*, 6381−6389.
(58) Chen, Y.; Chen, D.; Li, Z.; Peng, X. Symmetry-Breaking for Formation of Rectangular CdSe Two-Dimensional Nanocrystals in Zinc-Blende Structure. *J. Am. Chem. Soc.* **2017**, *139*, 10009−10019.
(59) Riedinger, A.; Ott, F. D.; Mule, A.; Mazzotti, S.; Knüsel, P. N.; Kress, S. J. P.; Prins, F.; Erwin, S. C.; Norris, D. J. An Intrinsic Growth Instability in Isotropic Materials Leads to Quasi-Two-Dimensional Nanoplatelets. *Nat. Mater.* **2017**, *16*, 743−748.
(60) Li, Z.; Qin, H.; Guzun, D.; Benamara, M.; Salamo, G.; Peng, X. Uniform Thickness and Colloidal-Stable CdS Quantum Disks with Tunable Thickness: Synthesis and Properties. *Nano Res.* **2012**, *5*, 337−351.
(61) Tang, Z.; Kotov, N. A.; Giersig, M. Spontaneous Organization of Single CdTe Nanoparticles into Luminescent Nanowires. *Science* **2002**, *297*, 237−240.
(62) Oh, S. J.; Uswachoke, C.; Zhao, T.; Choi, J.-H.; Diroll, B. T.; Murray, C. B.; Kagan, C. R. Selective p- and n-Doping of Colloidal PbSe Nanowires To Construct Electronic and Optoelectronic Devices. *ACS Nano* **2015**, *9*, 7536−7544.
(63) Cho, K. S.; Talapin, D. V.; Gaschler, W.; Murray, C. B. Designing PbSe Nanowires and Nanorings through Oriented Attachment of Nanoparticles. *J. Am. Chem. Soc.* **2005**, *127*, 7140−7147.
(64) van Huis, M. A.; Kunneman, L. T.; Overgaag, K.; Xu, Q.; Pandraud, G.; Zandbergen, H. W.; Vanmaekelbergh, D. Low-Temperature Nanocrystal Unification through Rotations and Relaxations Probed by *in-Situ* Transmission Electron Microscopy. *Nano Lett.* **2008**, *8*, 3959−3963.
(65) Groeneveld, E.; van Berkum, S.; Meijerink, A.; de Mello Donegá, C. Growth and Stability of ZnTe Magic Size Nanocrystals. *Small* **2011**, *7*, 1247−1256.
(66) Tang, Z.; Zhang, Z.; Wang, Y.; Glotzer, S. C.; Kotov, N. A. Self-Assembly of CdTe Nanocrystals into Free-Floating Sheets. *Science* **2006**, *314*, 274−278.
(67) Srivastava, S.; Santos, A.; Critchley, K.; Kim, K.-S.; Podsiadlo, P.; Sun, K.; Lee, J.; Xu, C.; Lilly, G. D.; Glotzer, S. C.; Kotov, N. A. Light-Controlled Self-Assembly of Semiconductor Nanoparticles into Twisted Ribbons. *Science* **2010**, *327*, 1355−1359.
(68) Bielewicz, T.; Dogan, S.; Klinke, C. Tailoring the Height of Ultrathin PbS Nanosheets and Their Application as Field-Effect Transistors. *Small* **2015**, *11*, 826−833.
(69) Khan, A. H.; Brescia, R.; Polovitsyn, A.; Angeloni, I.; Martín-García, B.; Moreels, I. Near-Infrared Emitting Colloidal PbS Nanoplatelets: Lateral Size Control and Optical Spectroscopy. *Chem. Mater.* **2017**, *29*, 2883−2889.
(70) Boneschanscher, M. P.; Evers, W. H.; Geuchies, J. J.; Altantzis, T.; Goris, B.; Rabouw, F. T.; van Rossum, S. A. P.; van der Zant, H. S. J.; Siebbeles, L. D. A.; Van Tendeloo, G.; et al. Long-Range Orientation and Atomic Attachment of Nanocrystals in 2D Honeycomb Superlattices. *Science* **2014**, *344*, 1377−1380.
(71) Geuchies, J. J.; van Overbeek, C.; Evers, W. H.; Goris, B.; de Backer, A.; Gantapara, A. P.; Rabouw, F. T.; Hilhorst, J.; Peters, J. L.; Konovalov, O.; et al. *In Situ* Study of the Formation Mechanism of Two-Dimensional Superlattices from PbSe Nanocrystals. *Nat. Mater.* **2016**, *15*, 1248−1255.
(72) Whitham, K.; Yang, J.; Savitzky, B. H.; Kourkoutis, L. F.; Wise, F.; Hanrath, T. Charge Transport and Localization in Atomically Coherent Quantum Dot Solids. *Nat. Mater.* **2016**, *15*, 557−564.
(73) van der Stam, W.; Gantapara, A. P.; Akkerman, Q. A.; Soligno, G.; Meeldijk, J. D.; van Roij, R.; Dijkstra, M.; de Mello Donega, C. d. M. Self-Assembly of Colloidal Hexagonal Bipyramid- and Bifrustum-shaped ZnS Nanocrystals into Two-Dimensional Superstructures. *Nano Lett.* **2014**, *14*, 1032−1037.
(74) van der Stam, W.; Rabouw, F. T.; Vonk, S. J. W.; Geuchies, J. J.; Ligthart, H.; Petukhov, A. V.; de Mello Donega, C. d. M. Oleic Acid Induced Atomic Alignment of ZnS Polyhedral Nanocrystals. *Nano Lett.* **2016**, *16*, 2608−2614.
(75) Fiori, G.; Bonaccorso, F.; Iannaccone, G.; Palacios, T.; Neumaier, D.; Seabaugh, A.; Banerjee, S. K.; Colombo, L. Electronics Based on Two-Dimensional Materials. *Nat. Nanotechnol.* **2014**, *9*, 768−779.
(76) Akinwande, D.; Petrone, N.; Hone, J. Two-Dimensional Flexible Nanoelectronics. *Nat. Commun.* **2014**, *5*, 5678.
(77) de Mello Donega, C. d. M. Formation of Nanoscale Spatially Indirect Excitons: Evolution of the Type-II Optical Character of CdTe/CdSe Heteronanocrystals. *Phys. Rev. B: Condens. Matter Mater. Phys.* **2010**, *81*, 165303.
(78) de Mello Donega, C.; Koole, R. Size Dependence of the Spontaneous Emission Rate and Absorption Cross Section of CdSe and CdTe Quantum Dots. *J. Phys. Chem. C* **2009**, *113*, 6511−6520.
(79) Ithurria, S.; Tessier, M. D.; Mahler, B.; Lobo, R. P. S. M.; Dubertret, B.; Efros, A. L. Colloidal Nanoplatelets with Two-Dimensional Electronic Structure. *Nat. Mater.* **2011**, *10*, 936−941.
(80) Wayman, V. L.; Morrison, P. J.; Wang, F.; Tang, R.; Buhro, W. E.; Loomis, R. A. Bound 1D Excitons in Single CdSe Quantum Wires. *J. Phys. Chem. Lett.* **2012**, *3*, 2627−2632.
(81) Zhou, Y.; Wang, F.; Buhro, W. E. Large Exciton Energy Shifts by Reversible Surface Exchange in 2D II−VI Nanocrystals. *J. Am. Chem. Soc.* **2015**, *137*, 15198−15208.
(82) Wise, F. W. Lead Salt Quantum Dots: the Limit of Strong Quantum Confinement. *Acc. Chem. Res.* **2000**, *33*, 773−780.
(83) Protesescu, L.; Yakunin, S.; Bodnarchuk, M. I.; Krieg, F.; Caputo, R.; Hendon, C. H.; Yang, R. X.; Walsh, A.; Kovalenko, M. V. Nanocrystals of Cesium Lead Halide Perovskites ($CsPbX_3$, X= Cl, Br, and I): Novel Optoelectronic Materials Showing Bright Emission with Wide Color Gamut. *Nano Lett.* **2015**, *15*, 3692−3696.
(84) Weidman, M. C.; Seitz, M.; Stranks, S. D.; Tisdale, W. A. Highly Tunable Colloidal Perovskite Nanoplatelets through Variable Cation, Metal, and Halide Composition. *ACS Nano* **2016**, *10*, 7830−7839.
(85) Xu, Y. Q.; Chen, Q.; Zhang, C. F.; Wang, R.; Wu, H.; Zhang, X.; Xing, G.; Yu, W. W.; Wang, X.; Zhang, Y.; et al. Two-Photon-Pumped Perovskite Semiconductor Nanocrystal Lasers. *J. Am. Chem. Soc.* **2016**, *138*, 3761−3768.
(86) Zhang, X. Y.; Lin, H.; Huang, H.; Reckmeier, C.; Zhang, Y.; Choy, W. C. H.; Rogach, A. L. Enhancing the Brightness of Cesium Lead Halide Perovskite Nanocrystal Based Green Light-Emitting Devices through the Interface Engineering with Perfluorinated Ionomer. *Nano Lett.* **2016**, *16*, 1415−1420.
(87) Swarnkar, A.; Marshall, A. R.; Sanehira, E. M.; Chernomordik, B. D.; Moore, D. T.; Christians, J. A.; Chakrabarti, T.; Luther, J. M. Quantum Dot-Induced Phase Stabilization of Alpha-$CsPbI_3$ Perovskite for High-Efficiency Photovoltaics. *Science* **2016**, *354*, 92−95.
(88) van der Stam, W.; Geuchies, J. J.; Altantzis, T.; van den Bos, K. H. W.; Meeldijk, J. D.; Van Aert, S.; Bals, S.; Vanmaekelbergh, D.; de Mello Donega, C. Highly Emissive Divalent Ion Doped Colloidal $CsPb_{1-x}M_xBr_3$ Perovskite Nanocrystals through Cation Exchange. *J. Am. Chem. Soc.* **2017**, *139*, 4087−4097.
(89) Yu, Y.; Zhang, D.; Kisielowski, C.; Dou, L.; Kornienko, N.; Bekenstein, Y.; Wong, A. B.; Alivisatos, A. P.; Yang, P. Atomic Resolution Imaging of Halide Perovskites. *Nano Lett.* **2016**, *16*, 7530−7535.

DOI: 10.1021/acs.jpclett.7b01640
J. Phys. Chem. Lett. 2017, 8, 4077−4090